

# Deflection versus penetration of a wedge-loaded crack: effects of branch-crack length and penetrated-layer width<sup>☆</sup>

M.Y. He<sup>a</sup>, C.H. Hsueh<sup>b,\*</sup>, P.F. Becher<sup>b</sup>

<sup>a</sup>Materials Department, University of California, Santa Barbara, CA 93106-5050, USA

<sup>b</sup>Metals and Ceramics Division, Oak Ridge National Laboratory, Oak Ridge, TN 37831-6068, USA

Received 9 September 1999; accepted 24 December 1999

## Abstract

A crack intersecting an interface between two dissimilar material layers may advance by either deflecting along or penetrating through the interface. The criterion of deflection versus penetration can be established by the comparison of two ratios, the energy release rate ratio and the fracture energy ratio, of deflection to penetration. The effects of: (1) a finite length of the branch crack emanating from the main crack tip; and (2) a finite width of the layer subjected to crack penetration were examined in the present study. The results reveal that the above two factors have profound effects on the criterion of deflection versus penetration for a wedge-loaded crack. © 2000 Elsevier Science Ltd. All rights reserved.

*Keywords:* A. Layered structures; B. Debonding; C. Finite element analysis (FEA)

## 1. Introduction

In an earlier paper by He and Hutchinson [1], a study was made on the tendency of a wedge-loaded crack meeting a bimaterial interface to either deflect along the interface or penetrate through the interface into the next layer. The analysis was conducted in terms of the energy release rate ratio of crack deflecting into the interface,  $G_d$ , to crack penetrating through the interface,  $G_p$ . The criterion of deflection versus penetration was then established depending on whether  $G_d/G_p$  was greater or less than the ratio of the fracture energy of the interface  $\Gamma_i$  to that of the adjoining layer,  $\Gamma_f$ . This criterion has been adopted extensively to predict interfacial debonding versus reinforcement fracture for fiber- (whisker- and self-) reinforced ceramic composites. However, due to the assumptions made in the asymptotic analysis, in which integral equation methods were used, two limitations should be noted before the criterion is applied. First, the results were obtained based on the

condition that the branch crack emanating from the main crack tip was very small compared with all other lengths in the problem; including the length of the main crack itself. Second, the analysis was for two semi-infinite elastic materials bonded at the interface. For the crack initiation problem, the branch crack can be treated as an infinitely small crack; therefore, these two assumptions are satisfied. However, in some cases (e.g. for a wedge-loaded crack, or in the presence of residual stresses), the length of the branch crack becomes an important parameter, and these two conditions are not satisfied. The effects of the finite branch-crack length may well be significant.

Recently, the bonding strength at the whisker/glass interface in a model composite of oxynitride glass matrix containing 5 vol%  $\beta$ - $\text{Si}_3\text{N}_4$  whiskers has been evaluated by an indentation-induced crack-deflection method [2,3]. A cube-corner indenter was used to generate a crack in the glass. When the crack intersects the whisker, it will either deflect at the interface propagating a finite length and then kinking into the whisker or penetrate the whisker. In this case, the branch crack has a finite length and the whisker subjected to crack penetration has a finite width.

As an initial attempt to analyze the indentation-induced crack-deflection problem in the whisker/glass system and as a complement to the previous study [1], the present study sought to examine effects of: (1) a finite length of the branch crack emanating from the main crack tip; and (2) a finite

<sup>☆</sup> This manuscript has been authorized by a contractor of the US Government, under contract no. DE-ACO596OR22464. Accordingly, the US Government retains a nonexclusive, royalty-free license to publish or reproduce the published form of this contribution, or allow others to do so, for US Government purposes.

\* Corresponding author. Tel.: + 1-423-576-6586; fax: + 1-423-574-8445.

E-mail address: hsuehc@ornl.gov (C.H. Hsueh).

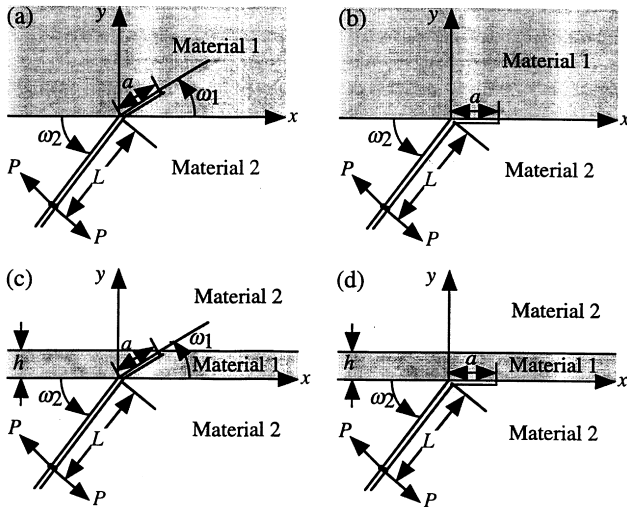


Fig. 1. Schematic drawings showing: (a) a penetrating crack; and (b) a deflected crack for two semi-infinite dissimilar materials bonded at the interface; and (c) a penetrating crack; and (d) a deflected crack for material 1 with a width,  $h$ , sandwiched between two semi-infinite material 2.

width of the adjoining layer subjected to crack penetration on the criterion of crack deflection versus penetration. To achieve this, integral equation methods were not feasible because of the complication of the problem and the finite element method was hence adopted. First, to verify the accuracy of the finite element method, solutions were compared to those obtained from Muskhelishvili's method [4] and integral equation methods [1], respectively, for two special cases. Then, using the finite element method, the effects of the branch-crack length and the penetrated-layer width were examined. It is noted that the related problems with different geometries have been examined by a number of researchers. For example, the tendency of a crack to deflect or penetrate at an interface between two dissimilar elastic materials in a double-edged notch specimen [5] and the effect of flaws [6] have been investigated using the boundary element method. Recently Bush [7] studied the effects of a pre-existing flaw on the interface of a particle on the crack propagation.

## 2. The system

Schematic drawings of crack penetration and deflection for an oblique wedge-loaded crack used in the previous study [1] are shown in Fig. 1a and b, respectively. Two semi-infinite elastic materials, material 1 and material 2, are bonded at the interface. The main crack in material 2 is subjected to wedge opening loads,  $P$ , at a distance,  $L$ , from the interface along the crack line. The crack intersects the interface at an oblique angle,  $\omega_2$ , and can either penetrate across the interface into material 1 or deflect at the interface. The resultant branch crack has a length  $a$ . For the case of a penetrating crack (Fig. 1a), the angle between

the branch crack and the interface is  $\omega_1$ . To examine the effects of a finite length of the branch crack, the problems were solved for finite values of  $a/L$ . To examine the effects of a finite width of material 1, a layer of material 1 with a width,  $h$ , sandwiched between two semi-infinite material 2 was considered, and the schematic drawings for crack penetration and deflection are shown, respectively, in Fig. 1c and d.

For the plane-strain bimaterial problem, the solution variables of interest depend on two non-dimensional elastic mismatch parameters; i.e. the Dundurs' parameters [8] which are

$$\alpha = (\bar{E}_1 - \bar{E}_2)/(\bar{E}_1 + \bar{E}_2) \quad (1)$$

$$\beta = \frac{1}{2}[\mu_1(1 - 2\nu_2) - \mu_2(1 - 2\nu_1)]/[\mu_1(1 - \nu_2) + \mu_2(1 - \nu_1)] \quad (2)$$

where  $E$ ,  $\mu$  and  $\nu$  are Young's modulus, shear modulus and Poisson's ratio, respectively,  $\bar{E} = E/(1 - \nu^2)$ , and the subscripts 1 and 2 denote materials 1 and 2, respectively. Since experience with related problems suggests that  $\alpha$  is the much more important one of the two parameters, the role of  $\alpha$  is emphasized and  $\beta = 0$  is taken in the present study.

## 3. Analyses

The finite element method was used in the present study to analyze: (1) the energy release rates for a deflected crack and a penetrating crack; and (2) the stress intensity factors and, hence, the mode mixity for a deflected crack. While the comparison of the energy release rate ratio to the fracture energy ratio of a deflected crack to a penetrating crack defines the criterion of crack deflection versus penetration, the mode mixity of a deflected crack characterizes the tendency for the deflected crack to kink into the adjoining layer.

### 3.1. The energy release rates and stress intensity factors

The solutions for the stress intensity factors for the problem of a penetrating crack depicted by Fig. 1a can be written as [1]

$$K_I + iK_{II} = c(\alpha, \omega_1, \omega_2, a/L)PL^{-1/2} \quad (3)$$

where  $i = \sqrt{-1}$ , and  $c$  is a dimensionless complex-valued function of the arguments indicated. The corresponding energy release rate,  $G_p$ , is

$$G_p = \frac{(1 - \nu_1)}{2\mu_1} |c|^2 \frac{P^2}{L} \quad (4)$$

It is noted that  $G_p$  is a function of  $\omega_1$ , and the maximum value of  $G_p$  with respect to  $\omega_1$  for a fixed  $a/L$  is denoted by  $G_p^{\max}$ .

The stress intensity factors for a deflected crack (Fig. 1b)

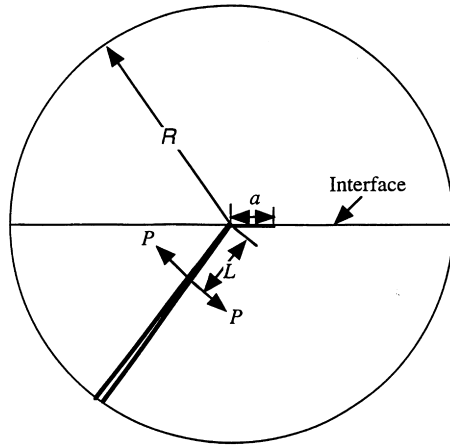


Fig. 2. A schematic drawing of the circular region adopted in the finite element calculation.

can be expressed by [1]

$$K_1 + iK_2 = d(\alpha, \omega_2, a/L)PL^{-1/2} \quad (5)$$

where  $d$  is a dimensionless complex-valued function of the arguments indicated. The corresponding energy release rate of the deflected crack,  $G_d$ , is given by

$$G_d = \frac{1}{\bar{E}^*} |d|^2 P^2 / L \quad (6)$$

where  $\bar{E}^*$  is given by

$$\frac{1}{\bar{E}^*} = \left[ \frac{1}{\bar{E}_1} + \frac{1}{\bar{E}_2} \right] \frac{1 - \beta^2}{2} \equiv \frac{1 - \beta^2}{(1 - \alpha)\bar{E}_1} \quad (7)$$

The ratio of the competing energy release rates is hence

$$\frac{G_d}{G_p^{\max}} = \frac{|d|^2}{(1 - \alpha)|c|^2} \quad (8)$$

### 3.2. The finite element method and convergence studies

The numerical results presented in this paper were computed using a finite element code, ABAQUS (Version 5.5) [9], with eight-node isoparametric elements. A quarter-point crack tip element served to model the inverse square root stress singularity at the crack tip. The model employed in the finite element calculation was a circular region with a radius  $R$  and its origin located at the intersection of the main crack and the interface (Fig. 2). In order to obtain the asymptotic solution,  $R$  should be much larger than both the length of the branch crack,  $a$ , and the distance from

Table 1

Errors of the strain energy release rate from the finite element solutions for meshing a circular region with a radius  $R$  for the system of an infinite plane containing a semi-infinite crack subjected to a point load at a distance  $L$  from the crack tip

$R/L$	200	400	1000	2500	5000
Error (%)	5.43	2.63	1.06	0.32	0.14

the wedge load to the crack tip,  $L$ . A refined mesh was used, and the detailed discussion of the finite element mesh can be found in the Appendix of Ref. [10]. For example, the mesh for the deflected crack contained 2499 eight-node isoparametric elements and 9339 nodes.

Two techniques were employed to calculate strain energy release rates. In the first, the  $J$ -integral was calculated by the domain integral method [11] for ten contours. In the second, the stress intensity factors  $K_1$  and  $K_2$  were obtained from the crack opening displacements,  $\delta_y$  and  $\delta_x$ , in accordance with (for  $\beta = 0$ )

$$K_1 = \lim_{r \rightarrow 0} \frac{E_1 \sqrt{\pi} \delta_y}{4\sqrt{2r}} \quad (9a)$$

$$K_2 = \lim_{r \rightarrow 0} \frac{E_1 \sqrt{\pi} \delta_x}{4\sqrt{2r}} \quad (9b)$$

The mode mixity,  $\psi$ , was then obtained, such that

$$\psi = \tan^{-1}(K_2/K_1) \quad (10)$$

It was found that the energy release rates obtained by these two methods were in very good agreement. The results for the energy release rate presented in this paper were obtained by  $J$ -integral, and the results for the mode mixity were obtained by the stress intensity factor method.

To ensure the convergence of the finite element solutions, results were compared to those obtained from Muskhelishvili's method and integral equation methods, respectively, for two special cases shown as follows.

#### 3.2.1. Comparison to Muskhelishvili's method

For an infinite plane containing a semi-infinite crack, which is subjected to a point load,  $P$ , at a distance  $L$  from the crack tip, the exact analytical solution for the stress intensity at the crack tip,  $K_1$ , has been derived using Muskhelishvili's method, such that [12]

$$K_1 = \frac{P}{\sqrt{2\pi L}} \quad (11a)$$

The corresponding strain energy release rate,  $G$ , is hence

$$G = \frac{p^2(1 - \nu^2)}{2\pi LE} \quad (11b)$$

Comparison of the finite element analysis using different ratios of  $R/L$  to the exact analytical solution (Eq. (11b)) is shown in Table 1. The results indicate that the ratio

Table 2

Comparison of energy release rate ratio  $G_d/G_p^{\max}$  between finite element solutions and integral equation solutions ( $a/L = 0.1$  and  $\omega_2 = 45^\circ$ )

$\alpha$	$G_d/G_p^{\max}$	
	Finite element	Integral equation
-0.5	0.637	0.639
-0.1	0.686	0.688
0.1	0.754	0.759

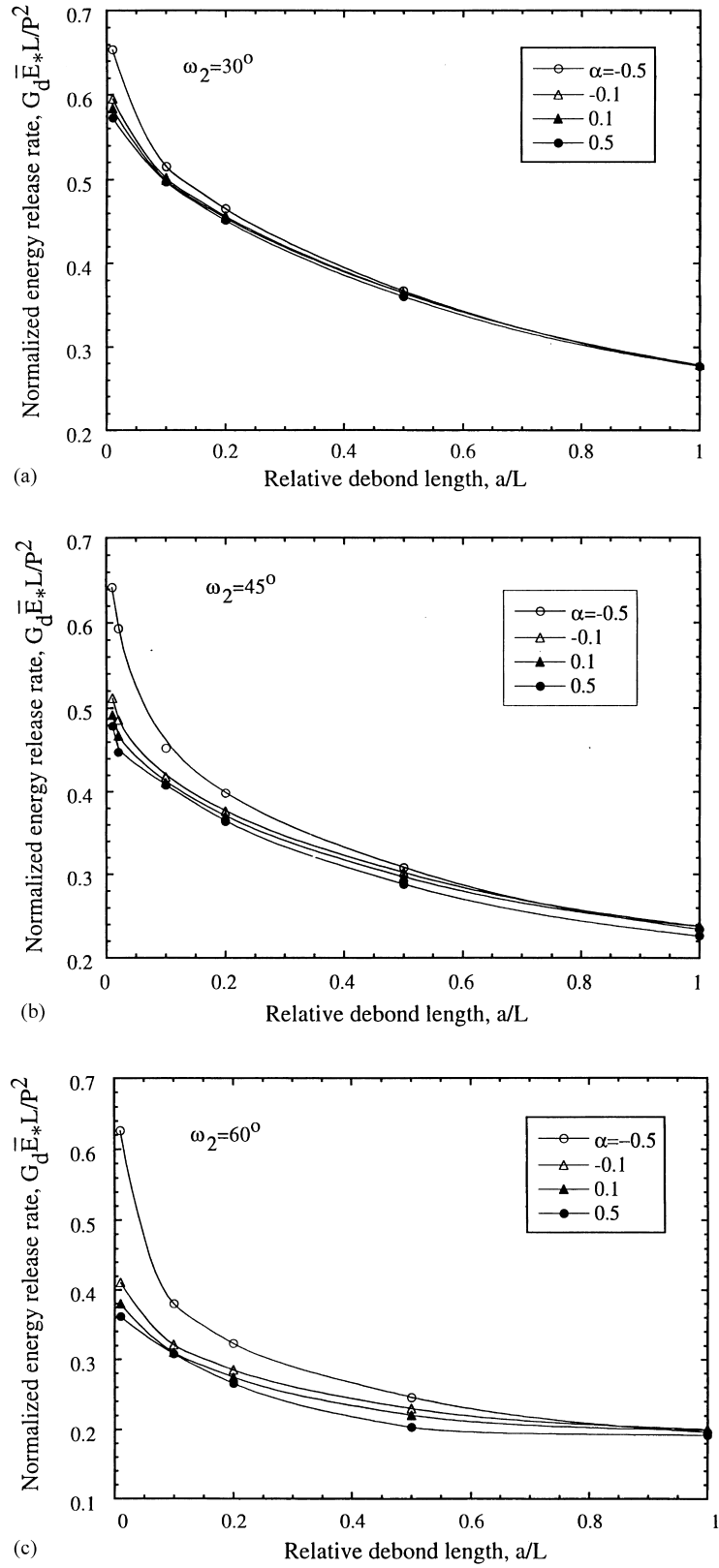


Fig. 3. The normalized energy release rate,  $G_d \bar{E}_* L / P^2$ , as a function of the relative debonding length,  $a/L$ , (a) for  $\omega_2 = 30^\circ$ , (b) for  $\omega_2 = 45^\circ$ , (c) for  $\omega_2 = 60^\circ$ .

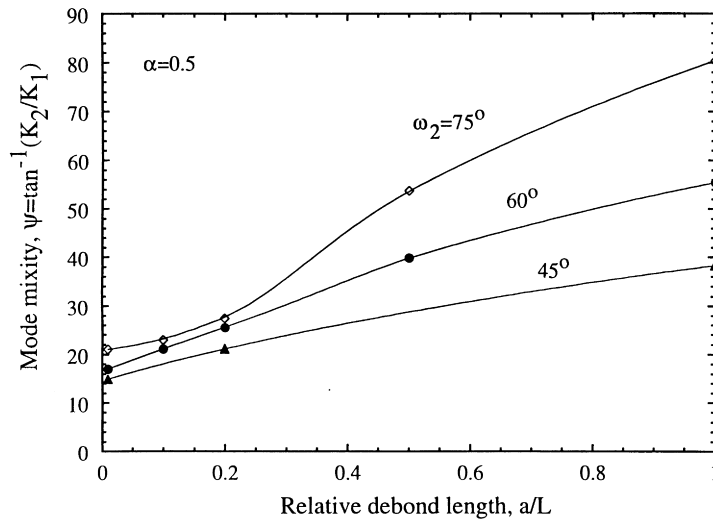


Fig. 4. The mode mixity,  $\psi$ , of the deflected crack as a function of the relative debonding length,  $a/L$ , for  $\alpha = 0.5$ .

$R/L = 1000$  is sufficient to obtain the asymptotic solutions. Hence,  $R/L$  ratios  $\geq 1000$  were used in the present finite element analysis.

### 3.2.2. Comparison to integral equation methods

For a penetrating crack (Fig. 1a), the energy release rate ratio  $G_d/G_p^{\max}$  as a function of  $\alpha$  has been calculated using integral equation methods for  $a/L = 0.1$  and  $\omega_2 = 45^\circ$  [1]. Using finite element analyses in the present study, results were also obtained and excellent agreement was found when comparing these values to those obtained from integral equation methods (see Table 2).

## 4. Results

In glass matrix containing whiskers, a deflected crack is

found to propagate a finite length along the interface before it kinks into the whisker [2,3]. In the following, the effects of the debond length on the energy release rate and the mode mixity of a deflected crack were examined first. Then, the effects of both a finite length of the branch crack emanating from the main crack tip and a finite width of the adjoining layer subjected to crack penetration on the criterion of crack deflection versus penetration were studied.

### 4.1. Effects of the debond length on the energy release rate and mode mixity of a deflected crack

For the geometry depicted in Fig. 1a, the normalized energy release rate of a deflected crack,  $G_d \bar{E}^* L/P^2 = |d|^2$ , as a function of the relative debond length,  $a/L$ , is plotted in Fig. 3a–c, respectively, for  $\omega_2 = 30, 45$  and  $60^\circ$  at different values of  $\alpha$ . The energy release rate,  $G_d$ , decreases as the

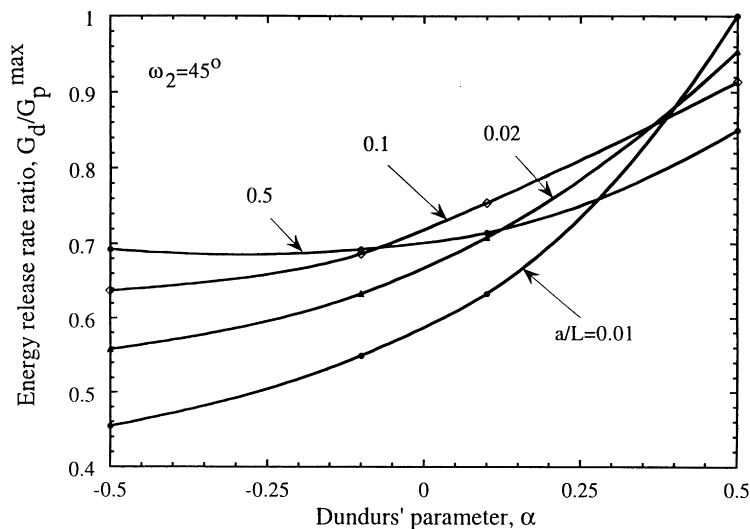


Fig. 5. The energy release rate ratio,  $G_d/G_p^{\max}$ , as a function of the Dundurs' parameter,  $\alpha$ , at different lengths of the branch crack for  $\omega_2 = 45^\circ$ .

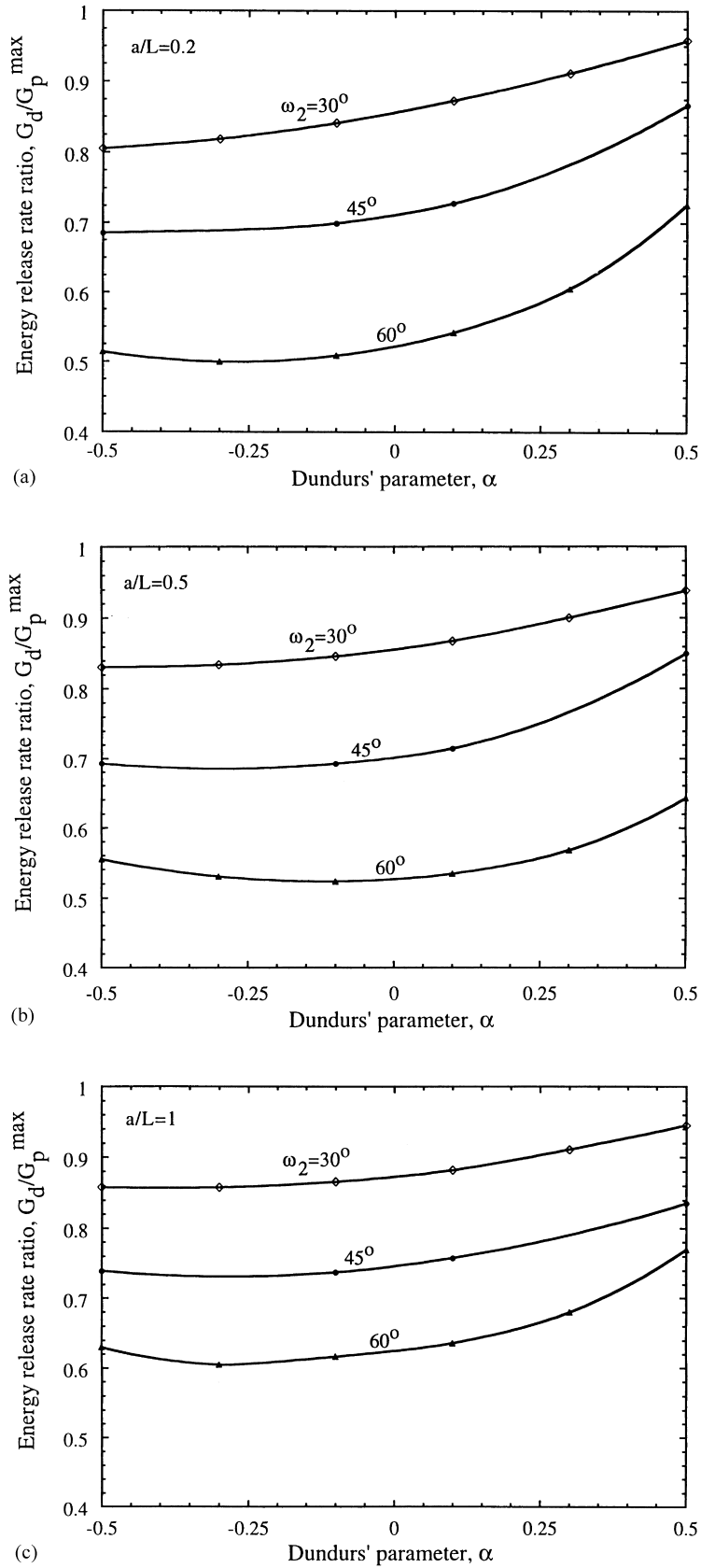


Fig. 6. The energy release rate ratio,  $G_d/G_p^{\max}$ , as a function of the Dundurs' parameter,  $\alpha$ , at different oblique angles,  $\omega_2$ : (a) for  $a/L = 0.2$ ; (b) for  $a/L = 0.5$ ; (c) for  $a/L = 1$ .

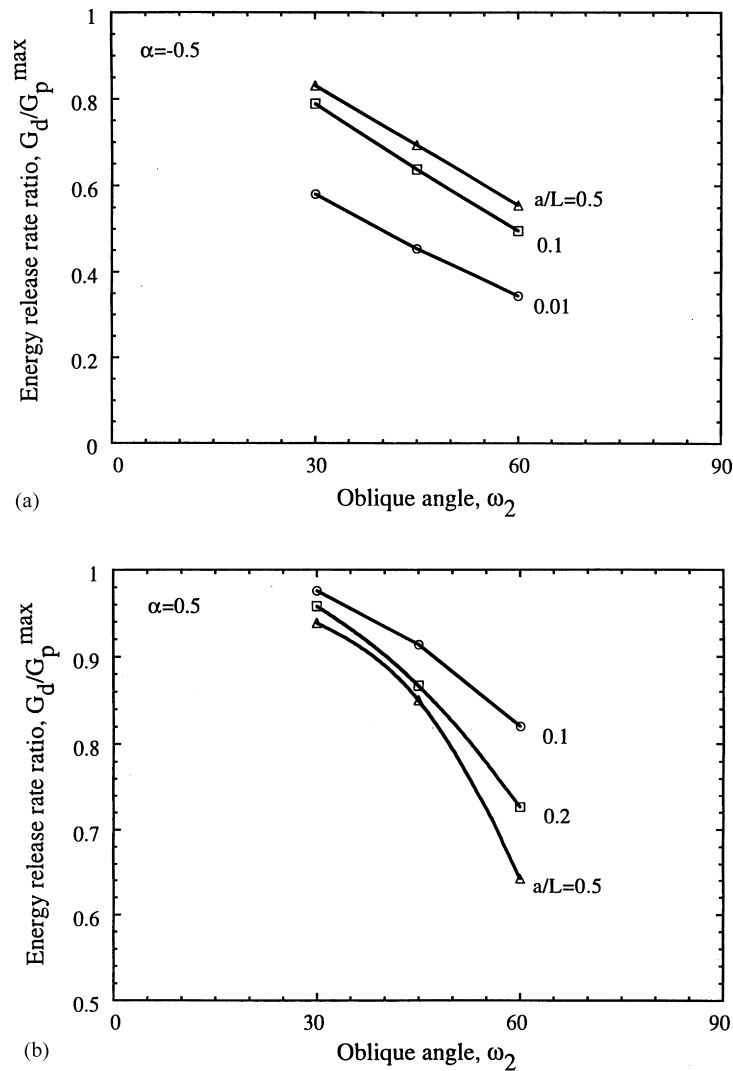


Fig. 7. The energy release rate ratio,  $G_d/G_p^{\max}$ , as a function of the oblique angle,  $\omega_2$ : (a) for  $\alpha = -0.5$ ; (b) for  $\alpha = 0.5$ .

debond length,  $a$ , increases. However, the elastic mismatch parameter,  $\alpha$ , has only a secondary effect on the normalized energy release rate. The associated mode mixity,  $\psi$ , of the deflected crack as a function of the relative debond length,  $a/L$ , is given in Fig. 4 for  $\alpha = 0.5$  at different oblique angles,  $\omega_2$ . The results show that the mode mixity,  $\psi$ , increases with increase in both the debond length and the oblique angle. Hence, based on Figs. 3 and 4, the energy release rate  $G_d$  (and hence  $G_d/G_p^{\max}$ ) decreases and the mode mixity  $\psi$  increases as the deflected crack grows which, in turn, make it more likely that the deflected crack in the interface will kink into material 1. These results agree with experimental observations [2,3]. However, to quantitatively characterize the bonding strength at the whisker/glass interface from the deflected crack length,  $G_p^{\max}$  for a deflected crack to kink into material 1 should also be calculated. This involves two stress singularities in the finite element analysis and will be done in the future.

#### 4.2. Effects of the branch-crack length on the energy release rate ratio, $G_d/G_p^{\max}$

Using the geometries depicted in Fig. 1a and b, the energy release rate ratio,  $G_d/G_p^{\max}$ , as a function of  $\alpha$  is plotted in Fig. 5 at different lengths of the branch crack (from  $a/L = 0.01$  to 0.5) for  $\omega_2 = 45^\circ$ . It can be seen that the relative branch-crack length,  $a/L$ , has significant effects on the energy release rate ratio.

While  $G_d/G_p^{\max}$  as a function of  $\alpha$  (i.e. the criterion of crack deflection versus penetration) in an earlier work [1] was established for  $a/L = 0.1$ , curves of  $G_d/G_p^{\max}$  as a function of  $\alpha$  for  $\omega_2 = 30, 45$  and  $60^\circ$  are shown in Fig. 6a–c for  $a/L = 0.2, 0.5$  and 1.0, respectively. Curves of  $G_d/G_p^{\max}$  as a function of  $\omega_2$  at different ratios of  $a/L$  are shown in Fig. 7a and b, respectively, for  $\alpha = -0.5$  and 0.5. The energy release rate ratio,  $G_d/G_p^{\max}$ , decreases with the increase in the oblique angle,  $\omega_2$ . It can also be seen that effects of the

branch-crack length on the energy release rate ratio depend on  $\alpha$ . For  $\alpha = -0.5$  the ratio increases with the increasing branch-crack length (Fig. 7a). On the other hand, for  $\alpha = 0.5$ , the ratio decreases with the increasing crack length (Fig. 7b).

#### 4.3. Effects of a finite width of material 1

For ceramic composites, the reinforcement embedded in the matrix has a finite width. To examine the effects of the reinforcement width on the criterion of crack deflection versus penetration, simplified geometries depicted by Fig. 1c and d were adopted in the present study. The energy release rate ratio,  $G_d/G_p^{\max}$ , as a function of  $\alpha$  is plotted in Fig. 8 at different widths of the sandwiched layer (i.e. material 1) for  $\omega_2 = 30, 45, 60$  and  $75^\circ$  and  $a/L = 0.01$ . The curve for  $L/h = 0$  (i.e.  $h \rightarrow \infty$ ) is also included which was the result presented in the earlier work [1]. The results in Fig. 8 show that the curve becomes flatter as the width of material 1 decreases (i.e.  $L/h$  increases).

The results for  $\omega_2 = 45$  and  $60^\circ$  in Fig. 8 are, respectively, replotted in Fig. 9a and b, in which  $G_d/G_p^{\max}$  as a function of the main crack length to sandwiched layer width ratio,  $L/h$ , is plotted at different values of  $\alpha$ . When  $\alpha = 0$  (i.e. materials 1 and 2 are the same),  $G_d/G_p^{\max}$  is independent of the width of material 1. When  $\alpha > 0$  and  $\alpha < 0$ , the calculated  $G_d/G_p^{\max}$  decreases and increases, respectively, as the width of material 1 decreases (i.e.  $L/h$  increases).

## 5. Concluding remarks

By considering two semi-infinite elastic materials bonded at the interface, specific crack propagation problems have been previously analyzed [1]. When a crack reaches the

interface, the crack either deflects along the interface or penetrates into the next layer depending upon the ratio of energy release rate due to debonding to that due to crack penetration. This criterion has been used extensively to predict interfacial debonding versus reinforcement fracture for a crack propagating in fiber- (whisker- and self-) reinforced ceramic composites. However, two limitations should be noted before the criterion is applied. First, the results were obtained based on the condition that the branch crack emanating from the main crack tip was very small compared with the main-crack length. Second, the fiber has a finite width and is not semi-infinite in a two-dimensional sense.

The present study examined effects of: (1) a finite branch-crack length; and (2) a finite penetrated-layer width on the criterion of crack deflection versus penetration, and the following results were concluded.

1. For a deflected crack (Fig. 1b), the energy release rate decreases (Fig. 3) and the mode mixity,  $\psi$ , increases (Fig. 4) as the deflected crack grows. This would make it more favorable for the deflected crack in the interface to kink into the adjoining layer as the deflected crack grows longer.
2. The branch-crack length has effects on the energy release rate ratio of crack deflection to penetration,  $G_d/G_p^{\max}$  (Figs. 5 and 6). The energy release rate ratio,  $G_d/G_p^{\max}$ , can increase or decrease with the increase in the branch-crack length depending on the Dundurs' parameter,  $\alpha$  (Fig. 7a and b).
3. The penetrated-layer width has significant effects on the energy release rate ratio of crack deflection to penetration,  $G_d/G_p^{\max}$ . The diagram of crack deflection versus penetration (i.e.  $G_d/G_p^{\max}$  as a function of  $\alpha$ ) is shown in Fig. 8. Specifically,  $G_d/G_p^{\max}$  is independent of the width of the penetrated-layer only when  $\alpha = 0$  (Fig. 9),

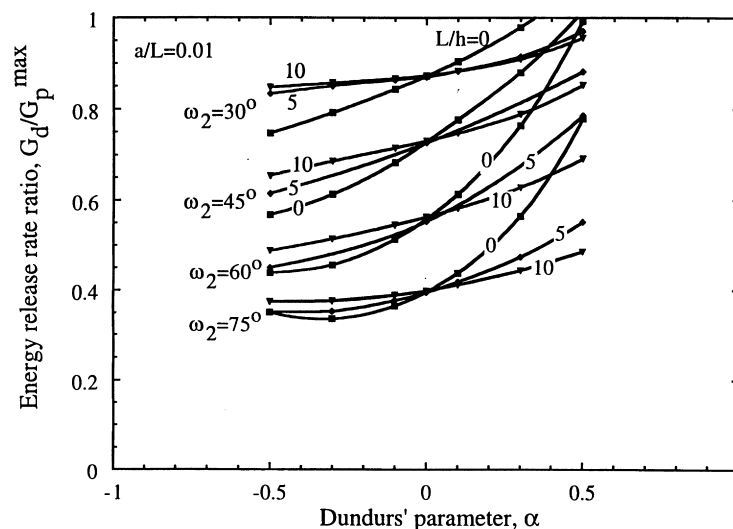


Fig. 8. The energy release rate ratio,  $G_d/G_p^{\max}$ , as a function of the Dundurs' parameter,  $\alpha$ , for  $a/L = 0.01$  at different values of  $L/h$  and  $\omega_2$ .

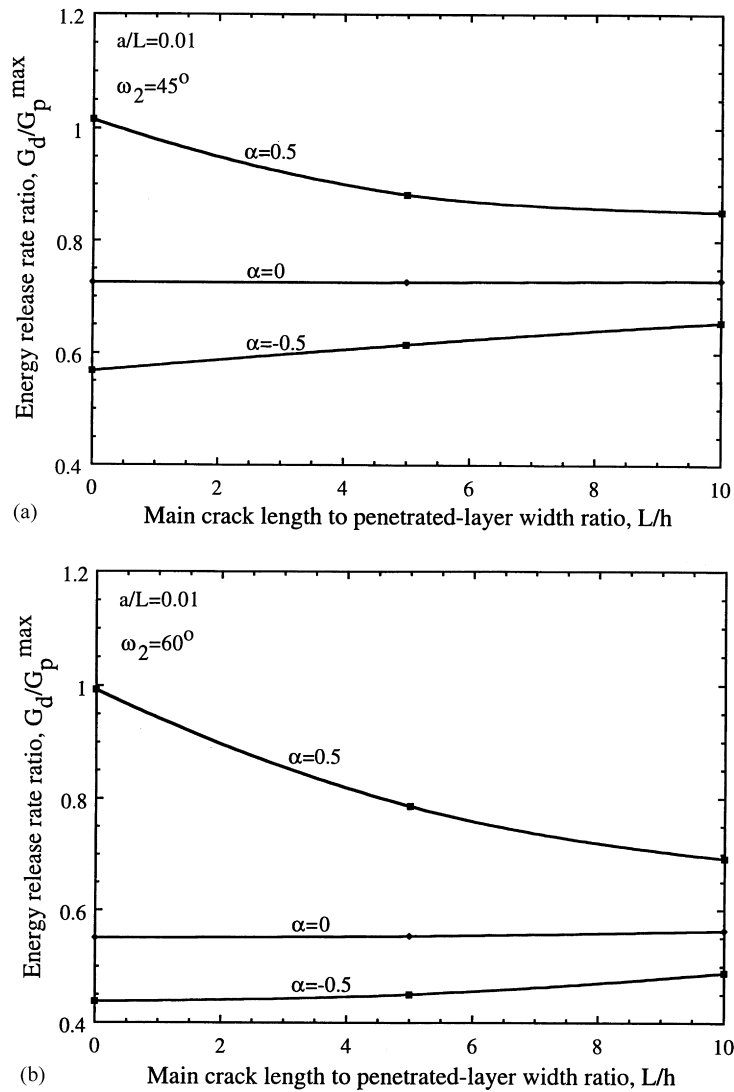


Fig. 9. The energy release rate ratio,  $G_d/G_p^{\max}$ , as a function of the main crack length to penetrated-layer width ratio,  $L/h$ , at different values of  $\alpha$ : (a) for  $\omega_2 = 45^\circ$ ; (b) for  $\omega_2 = 60^\circ$ .

and the curve in Fig. 8 becomes flatter as the width of the penetrated-layer (i.e. material 1 in Fig. 1c and d) decreases.

The present analysis is two-dimensional and is applicable to the layered materials. It should be noted that the crack propagation problem in fiber-reinforced composites is three-dimensional. For an embedded fiber of a finite radius, there are three options when a matrix crack reaches the interface: the interface can debond, the fiber can fracture, or the crack can circumvent the fiber. The present study considered a simplified geometry of material 1 with a finite width sandwiched between two semi-infinite material 2 (Fig. 1c and d), and hence focused on the case that the matrix crack does not circumvent the fiber. However, when the matrix crack circumvents the fiber, the crack is bridged by intact fibers, and the bridging-fiber (or fiber-pullout) geometry [13–15]

can be used as a representative volume element for this case. Considering a bridging fiber behind the crack tip,  $G_d/G_p^{\max}$  as a function of  $\alpha$  (for  $\omega_2 = 90^\circ$ ) has been derived elsewhere [16]. It is found that this ratio decreases with the increase in the Dundurs' parameter,  $\alpha$ . Also, the curve in the diagram of interfacial debonding versus fiber fracture becomes flatter as the fiber radius decreases [16].

#### Acknowledgements

The authors thank Dr M.J. Andrews and Dr M.J. Lance for reviewing the manuscript. Research sponsored by the US Department of Energy, Division of Materials Sciences, Office of Basic Energy Sciences, under contract DE-AC05-96OR22464 with Lockheed Martin Energy Research Corp.

## References

- [1] He MY, Hutchinson JW. Crack deflection at an interface between dissimilar elastic materials. *Int J Solids Struct* 1989;25(9):1053–67.
- [2] Becher PF, Hwang SL, Hsueh CH. Using microstructure to attack the brittle nature of silicon nitride ceramics. *MRS Bull Ser: Silicon-based Ceram* 1995;20:23–7.
- [3] Sun EY, Becher PF, Waters SB, Hsueh CH, Plucknett KP, Hoffmann MJ. Control of interface in silicon nitride ceramics: influence of different rare earth elements. In: Tomsia AP, Glaeser A, editors. *Ceramic Microstructures '96: Control at the atomic level*, New York: Plenum Press, 1998. p. 779–86.
- [4] Muskhelishvili NI. *Some basic problems of mathematical theory of elasticity*. Leiden: P. Noordhoff, 1953.
- [5] Tullock DL, Reimanis IE, Graham AL, Petrovic JJ. Deflection and penetration of cracks at an interface between two dissimilar materials. *Acta Metall Mater* 1994;42:3245–52.
- [6] Mammoli AA, Graham AL, Reimanis IE, Tullock DL. The effect of flaws on the propagation of cracks at bi-materials interfaces. *Acta Metall Mater* 1995;43:1149–56.
- [7] Bush MB. The interaction between a crack and a particle cluster. *Int J Fracture* 1998;88:215–32.
- [8] Dundurs J. Edge-bonded dissimilar orthogonal elastic wedge. *J Appl Mech* 1969;36:650–2.
- [9] ABAQUS Finite Element Code, Version 5.5, Hibbit, Karlsson and Sorensen, Inc., Pawtucket, RI.
- [10] He MY, Evans AG, Hutchinson JW. Crack deflection at an interface between dissimilar elastic materials: role of residual stresses. *Int J Solids Struct* 1994;31(24):3443–55.
- [11] Shih CF, Moran B, Nakamura J. Energy release rate along a three-dimensional crack front in a thermally stressed body. *Int J Fracture* 1986;30:79–102.
- [12] Tada H, Paris PC, Irwin GR. *The stress analysis of cracks handbook*. Paris Productions, 1985.
- [13] Gao YC, Mai YW, Cottrell B. Fracture of fiber-reinforced materials. *J Appl Math Phys* 1988;39(7):550–72.
- [14] McCartney LN. New theoretical model of stress transfer between fiber and matrix in a uniaxially fiber-reinforced composite. *Proc R Soc London A* 1989;425:215–44.
- [15] Hsueh CH. Interfacial debonding and fiber pull-out stresses of fiber-reinforced composites. *Mater Sci Engng A* 1990;123(1):1–11.
- [16] Hsueh CH, Becher PF. Interfacial shear debonding problems in fiber-reinforced ceramic composites. *Acta Mater* 1998;46(9):3237–45.